A cone-shaped 3D carbon nanotube probe for neural recording

Huan-Chieh Su [a], Chia-Min Lin [b], Shiang-Jie Yen [a], Yung-Chan Chen [c], Chang-Hsiao Chen [b], Shih-Rung Yeh [d], Weileun Fang [b], Hsin Chen [c], Da-Jeng Yao [b], Yen-Chung Chang [d], Tri-Rung Yew [a],*

[a] Department of Materials Science and Engineering, National Tsing Hua University, Hsinchu 30013, Taiwan
[b] Institute of NanoEngineering and MicroSystems, National Tsing Hua University, Hsinchu 30013, Taiwan
[c] Institute of Electronics Engineering, National Tsing Hua University, Hsinchu 30013, Taiwan
[d] Department of Life Sciences, National Tsing Hua University, Hsinchu 30013, Taiwan

ARTICLE INFO

ABSTRACT

A novel cone-shaped 3D carbon nanotube (CNT) probe is proposed as an electrode for applications in neural recording. The electrode consists of CNTs synthesized on the cone-shaped Si (cs-Si) tip by catalytic thermal chemical vapor deposition (CVD). This probe exhibits a larger CNT surface area with the same footprint area and higher spatial resolution of neural recording compared to planar-type CNT electrodes. An approach to improve CNT characteristics by O_2 plasma treatment to modify the CNT surface will be also presented. Electrochemical characterization of O_2 plasma-treated 3D CNT (OT-CNT) probes revealed low impedance per unit area ($\sim$64.5 Ω mm^{-2}) at 1 kHz and high specific capacitance per unit area ($\sim$2.5 mF cm^{-2}). Furthermore, the OT-CNT probes were employed to record the neural signals of a crayfish nerve cord. Our findings suggest that OT-CNT probes have potential advantages as high spatial resolution and superb electrochemical properties which are suitable for neural recording applications.

1. Introduction

Neurophysiologists use neural electrodes (NEs) to investigate the physiological functions of the brain. There are many traditional NEs, including penetrating electrodes, sharpened wire metal electrodes (Hubel, 1957; Loeb et al., 1995), the Michigan electrode (Wise, 2005) and the Utah electrode (Normann, 2007), which are used for the stimulation and recording of brain tissues, while cuff electrodes are implanted around peripheral nerves (Navarro et al., 2005; Keohan et al., 2007). Moreover, they are used for the treatment of numerous diseases, like Parkinson's disease, dystonia and chronic pain (Hochberg et al., 2006; Taylor et al., 2002; Chapin et al., 1999; Schwartz et al., 2006; Loeb et al., 1995). Despite the fact that NEs have been used successfully and demonstrated clinical relevance such as with deep brain stimulation (DBS) and cochlear implants, there are some challenges related to the utilization of NEs. For example, NEs are larger than single cells and exhibit excitation/recording areas extending 70–150 μm in all directions from the electrode. Additionally, they cause tissue and neural damage during implantation, and induce inflammatory responses upon long-term implantation. Hence, reducing NE size is a critical requirement (Kotov et al., 2009).

Si-based multi-microelectrode probes have been fabricated by the Micro-Electro-Mechanical System (MEMS) method to replace traditional NEs in the aspect of device structure improvement and device size scaling down (Campbell et al., 1990; Merabet et al., 2005; Patolsky et al., 2006; Lebedev and Nicolelis, 2006; Chen et al., 2009), and can enhance the spatial resolution of neural recording and stimulation. However, a significant reduction in electrode size greatly increases electrode impedance, limiting the recording sensitivity and the maximum stimulating current deliverable through an electrode. In order to resolve above issues, a reduction in electrode size must not sacrifice electrode function, and the impedance of the electrode must be as low as possible (Loeb et al., 1995; Kotov et al., 2009).

Carbon nanotubes (CNTs) exhibit intrinsically large surface areas (700–1000 m^2 g^{-1}) (Li et al., 2003), high mechanical strength (>1 TPa) (Krishnan et al., 1998), high electrical conductivity and intriguing physicochemical properties (Musameh et al., 2005; Shanmugam and Gedanken, 2006; Gooding, 2005). Hence, CNTs have become an attractive material for neuro-electronic interfaces (Lovat et al., 2005; Gheith et al., 2006; Mazzatenta et al., 2007). By growing CNTs on microelectrodes, the nanostructure of the CNTs inherently increases the effective interfacial area between the microelectrode and neuron (Wang et al., 2006; Gabay et al., 2007; Keefer et al., 2008). CNTs have also been demonstrated to be a biocompatible substrate that promotes neural growth, boosts neural activity (Lovat et al., 2005) and transmits electrical stimulation (Mazzatenta et al., 2007; Keefer et al., 2008). These promising

results have led to the fabrication of CNTs into microelectrodes or even microprobes for neural recording and stimulation.

In this work, novel cone-shaped (cs) 3D CNT probes were proposed for electrophysiological applications. The CNTs grown on the cs-Si tip by catalytic thermal chemical vapor deposition (CVD) as electrodes for extracellularly neural recording were investigated. In addition, O_2 plasma treatment has been proposed to change CNT surface characteristics from hydrophobic to hydrophilic to improve CNT wettability and electrical properties. The electrical properties of the O_2 plasma-treated 3D CNT (OT-CNT) probe and its application for the detection of action potential signals on crayfish were examined.

2. Materials and methods

2.1. Fabrication of cone-shaped (cs) 3D CNT probe

The fabrication processes of cone-shaped 3D CNT probe are illustrated in Fig. 1. An $n^+ \langle 1\,0\,0 \rangle$ silicon wafer with low resistivity (0.01–0.02 Ω cm) was deposited with Si_3N_4 (500 nm) by a low pressure chemical vapor deposition (LPCVD) system and spin coated with photoresist (PR) (Fig. 1a). The wafer was patterned with lithography and reactive ion etching (RIE) to leave the silicon nitride as a hard mask (please see the mask patterns in Supplemental information Fig. S1a) to resist wet etching (Fig. 1b). Isotropic Si etching with HF/nitric/acetic acid (HNA, 2:26:33 in volume) was used to form the cs-Si pad for the area with hard mask protection. The heights of the cs-Si pad were about 20–50 μm, and the bottom diameters of the cs-Si pad were about 40–100 μm depending on the size of the Si_3N_4 hard mask (Fig. 1c). A 1 μm SiO_2 film was deposited on the entire wafer by a plasma-enhanced chemical vapor deposition (PECVD) (Fig. 1d), followed by the spin-coating of photoresist (PR) (Fig. 1e). The tip of the cs-Si pad was patterned with lithography and the PR was removed by development. The cs-Si tip size was controlled by the patterns drawn on mask (please see the

mask patterns in Supplemental information Fig. S1b) and exposure time of photolithography process. The cs-Si was then etched with buffered oxide etch (BOE) to remove the SiO_2 without PR coating on the cs-Si tip (Fig. 1f). The Al (10 nm) and Fe (1 nm) catalysts were deposited sequentially onto the top of wafer by an electron evaporation system without breaking vacuum (Fig. 1g). The Al and Fe catalysts were removed except those on cs-Si tip by lift-off technique (Fig. 1h). Finally, CNTs were synthesized on the cs-Si tip with Al and Fe catalysts by catalytic thermal CVD to form a cone-shaped 3D CNT probe (Fig. 1i).

2.2. Carbon nanotube growth

CNTs were synthesized on cs-Si tips by catalytic thermal CVD using C_2H_2/H_2 as process gases and Fe as a catalyst. C_2H_2 (60 sccm) was used as the carbon source, H_2 (10 sccm) was used as a reduction gas to prevent oxidation of the catalyst, and Ar (200 sccm) was used as a carrier gas. The process pressure was maintained at 10 Torr. The growth temperature was varied at 400–800 °C to optimize the quality and density of CNTs on cs-Si tip to form 3D CNT probes. After CNT growth, the 3D CNT probes were treated by microwave (MW) treatment for 3 min at 900 W to improve the adhesion of CNTs onto the substrates (Su et al., 2010).

Scanning electron microscopy (SEM, JEOL 6500 and 7000) was employed to observe the morphology and structure of the 3D CNT probe. High-resolution transmission electron microscopy (HRTEM, JEOL JEM-2010) was utilized to analyze the CNT nanostructure.

Micro-Raman spectra (HORIBA JOBIN YVON, HR-800, laser excitation wavelength: 633 nm) were also used to measure the degree of graphitization for CNTs.

2.3. Electrochemical tests

The electrochemical properties of 3D CNT probes in phosphate buffered saline (PBS, pH = 7.4) solution were studied in a three elec-
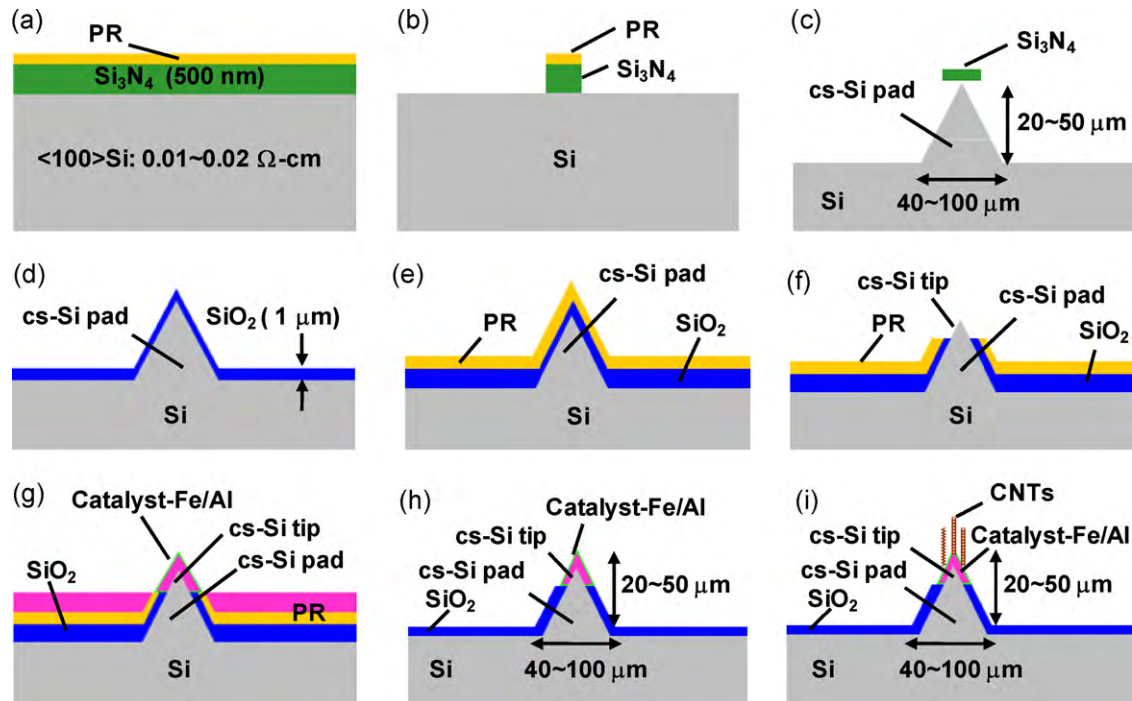

Fig. 1. Schematics of the fabrication process for cone-shaped (cs) 3D CNT probes. (a) Depositing 500 nm Si_3N_4 on a Si wafer with low resistivity (0.01–0.02 Ω cm) and spin-coating photoresist (PR), (b) PR patterning and reactive ion etching (RIE), (c) isotropic Si etching using HF/nitric/acetic acid to form the cs-Si pad, (d) depositing 1 μm SiO_2 on the top of the wafer, (e) spin-coating PR on the top of the wafer, (f) PR patterning and BOE etching to remove the SiO_2 without PR coating, (g) depositing Al (10 nm) and Fe (1 nm) catalysts, (h) using the lift-off process to remove the PR and catalyst on the area other than cs-Si tip, and (i) growing CNTs on the cs-Si tip by catalytic thermal CVD to form a cone-shaped 3D CNT probe.

trode configuration (CH Instruments, Model 680 Amp Booster). A Pt coil was used as the counter electrode, Ag/AgCl as the reference electrode, and the 3D CNT probe as the working electrode. Electrochemical impedance spectroscopy (EIS) was used to characterize the electrode–electrolyte interface impedance by applying a 10 mV AC signal with various frequencies (10 Hz–10 kHz) to the 3D CNT probe. In the cyclic voltammetry (CV) measurements, the potential was set at −0.3 to 0.6 V to avoid electrolysis of the PBS solution. The sweeping rate was 100 mV s^{-1}.

2.4. Neural electrophysiological experiments

Electrophysiological recording was performed according to procedures described previously (Yeh et al., 2009; Tseng et al., 2008). A crayfish was anesthetized in a 4 °C water bath, and the abdomen was cut from the thorax. The dorsal exoskeletons of segments from 1 to 5 were removed. The preparation was then pinned on Sylgard in a 4.5 cm diameter Petri dish containing crayfish saline (210 mM NaCl; 15 mM CaCl$_2$, 5.4 mM KCl, 2.6 mM MgCl$_2$ and 5 mM HEPES, pH 7.4). The 3D CNT probe was employed to record the neural activities of the lateral giant (LG) neuron in the crayfish, *Procambarus clarkia*. A 2.6 V square wave was input via a twisted Teflon-coated Ag wire to stimulate afferent fibers of the crayfish. The neural signal was recorded using the 3D CNT probe by pressing the electrodes against the LG axon. The recorded signals were digitalized at 100 kHz through a PCI-1602 A/D interface (ICP DAS, Taiwan). Subsequently, the digital data were stored and analyzed in a computer with a graphical-user-interface designed by the National Tsing Hua University, Taiwan.

3. Results and discussion

3.1. Physical characterization of the 3D CNT probe

A versatile 3D CNT probe with CNTs synthesized at 400–800 °C was fabricated for extracellular recording application. Although CNT growth at 400 °C was compatible with the complementary metal-oxide-semiconductor (CMOS) interconnect process, the length of the CNTs was short, and the density of the CNTs was not sufficient to cover the whole tip, as shown in Supplemental information Fig. S2. Therefore, the CNT growth at 800 °C was used as it can provide dense and long CNTs after serial experiments and process optimization. As shown in the SEM images in Fig. 2, the CNTs were self-assembled onto cs-Si tips with various sizes, including (a) 3.5 μm, (b) 16 μm and (c) 65 μm, which were precisely defined by the patterns drawn on the mask and photolithography process. The magnified SEM images (d), (e) and (f) show CNT grown on cs-Si tips taken from the boxed area in (a), (b) and (c), respectively.

The HRTEM image in Fig. 3a shows the as-grown multi-walled CNT (MWCNT) with amorphous carbon (a-C) on the CNT surface. The a-C was accumulated on the SiO$_2$ surface during the process of CNT growth at 800 °C. In addition to the influence of a-C on the CNT electrochemistry, a leakage current due to the conductance of a-C on SiO$_2$ area in the buffer solution occurred when using this 3D CNT probe (as-grown-CNT probe) for neural recording (see Section 3.3). Hence, O$_2$ plasma treatment was carried out to remove a-C from the SiO$_2$ and CNT surfaces of the 3D CNT probe. A plasma power of 50 W, 15 s etching time, 35 sccm O$_2$ process gas at 100 mTorr and at room temperature were found to be optimum a-C cleaning parameters. It was observed that excessive plasma power or longer etching time would cause CNT damage, while insufficient plasma power or etching time could not completely remove a-C. Fig. 3b shows the HRTEM image of the MWCNT with less a-C after O$_2$ plasma treatment. Moreover, the CNT surface changed from hydrophobic to hydrophilic, as shown by the contact angles of 146.3° (inset of Fig. 3a) and 3.5° (inset of Fig. 3b) before and after O$_2$ plasma treatment, respectively. The O$_2$ plasma treatment not only can remove a-C to avoid leakage current, but also can enhance the CNT hydrophilicity.

X-ray photoelectron spectroscopy (XPS) analyses were performed to investigate the changes of chemical concentration on CNTs, as shown Fig. 3c and d for as-grown and O$_2$ plasma treated CNTs (OT-CNTs), respectively. Both as-grown and O$_2$ plasma treated CNTs exhibit five peaks at 284.4 eV, 285.5 eV, 286.7 eV, 287.9 eV and 289.5 eV which are attributed to sp^2-hybridized C=C graphite, sp^3-hybridized C–C diamond-like, C–OH, C=O, and OH–C=O bonds, respectively (Li et al., 2007; Okpalugo et al., 2005). The relative percentages of C–OH, C=O and OH–C=O bonds for O$_2$ plasma treated CNTs (OT-CNTs) are slightly higher than those of
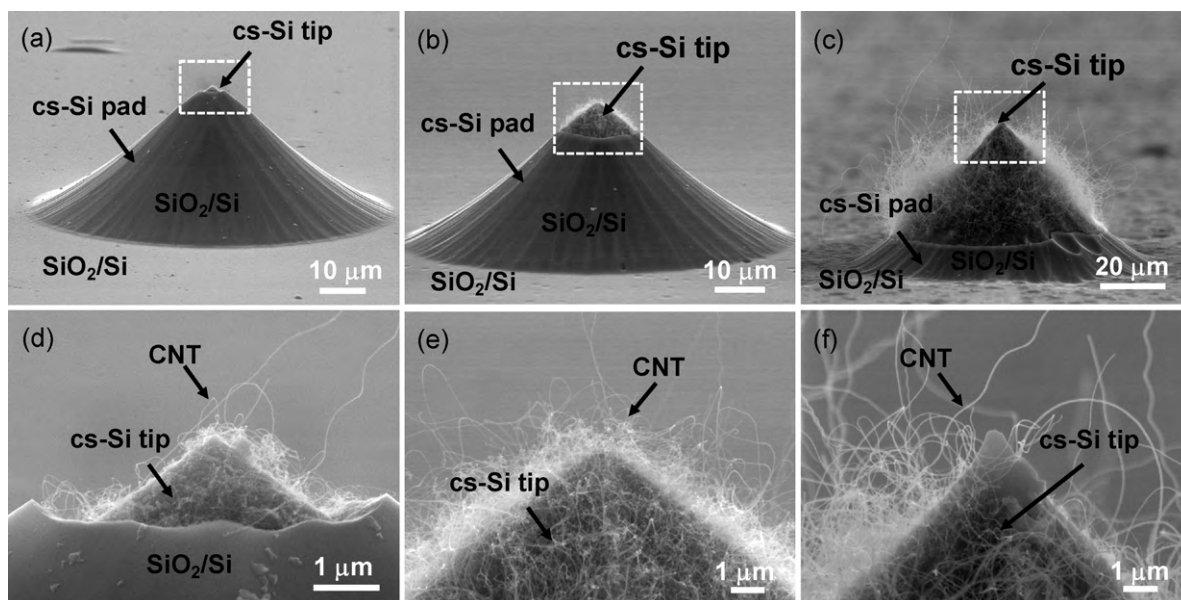

Fig. 2. SEM images showing the cs-Si tip with various sizes of CNT probes, including (a) 3.5 μm, (b) 16 μm and (c) 65 μm. The (d), (e), and (f) show magnified SEM images of the boxed area of (a), (b) and (c), respectively.
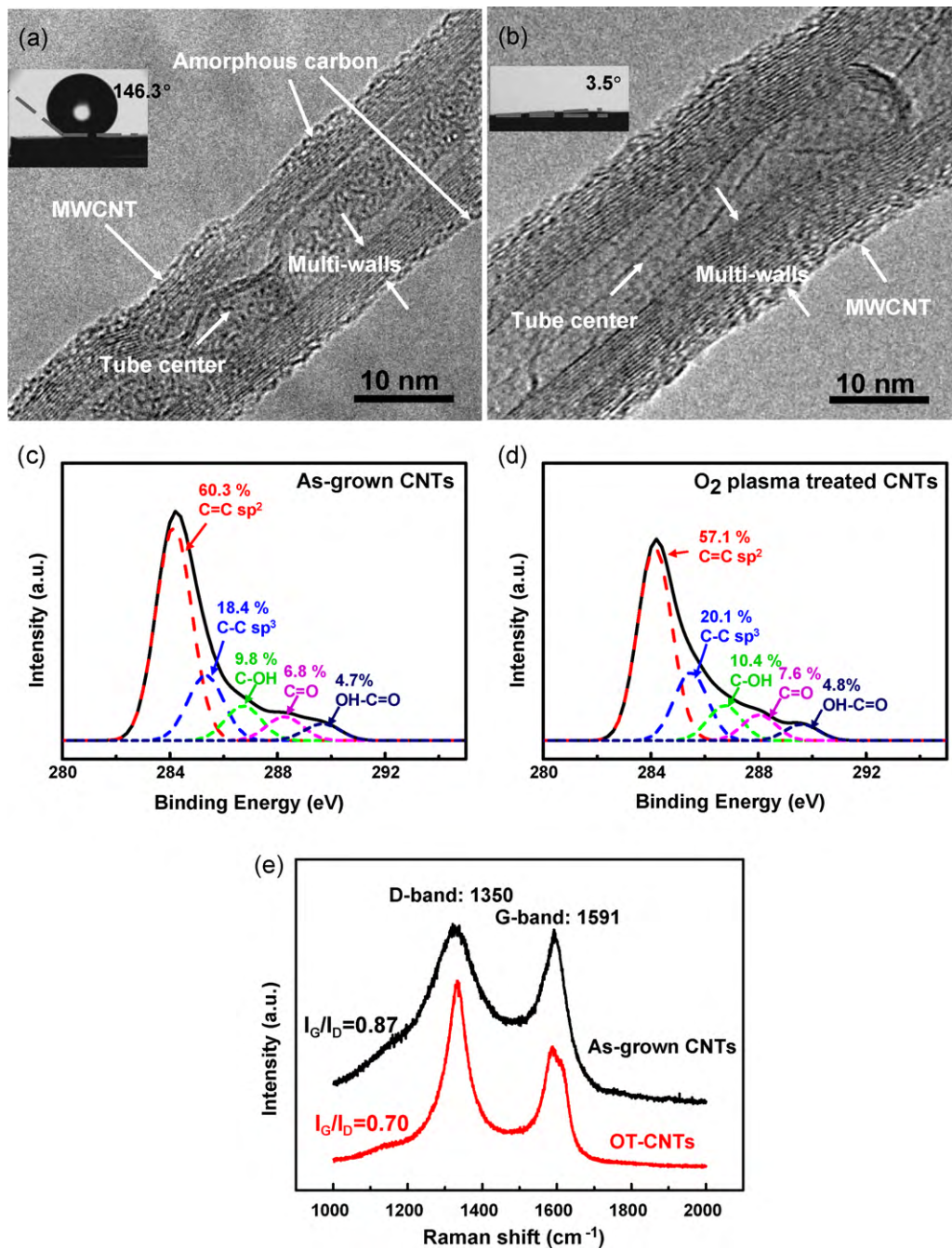
Fig. 3. High-resolution TEM images showing (a) the existence of a MWCNT with amorphous carbon (a-C) on the side wall before O$_2$ plasma treatment, and (b) MWCNT without a-C on the side wall after O$_2$ plasma treatment. The insets in (a) and (b) show the contact angle of as-grown CNTs and OT-CNTs, respectively. Gaussian decompositions of C 1s spectra of (c) as-grown CNTs and (d) O$_2$ plasma treated CNTs (OT-CNTs). (e) The Raman spectra of as-grown CNTs and O$_2$ plasma treated CNTs (OT-CNTs).

as-grown CNTs. It is possible that the formation of hydrophilic chemical bonds such as C–OH, C=O and OH–C=O on the outermost surface of the CNTs (Li et al., 2007) was enhanced by O$_2$ plasma treatment. Furthermore, Raman spectra were used to characterize the graphitization of as-grown CNTs and OT-CNTs, as shown in Fig. 3e. The sharper full width half maximum (FWHM) of the D-band after O$_2$ plasma treatment could be attributed to the reduction of a-C on the CNT surface (Lee et al., 2005). In addition, the G-band to D-band intensity ratio (G/D ratio, I_G/I_D) is about 0.87 for as-grown CNTs and 0.70 for OT-CNTs, indicating a slightly lower degree of graphitization of OT-CNTs. The lower G/D ratio indicates more defects on the CNTs (Endo et al., 2001).

3.2. Electrochemical characterization of the 3D CNT probe

The interfacial properties between the CNTs and electrolyte, which play an important role in neural signal detection, can be determined by EIS. Analyses of electrochemical impedance were used to obtain the impedance and the phase between the 3D CNT probes and the reference electrode. Fig. 4a and b shows the measured magnitude of impedance per unit area and the phase versus frequency, respectively, over the range of 10 Hz–10 kHz for the 3D probes without CNTs, with as-grown CNTs, and with OT-CNTs. The impedance per unit area dropped more than seven-fold for the probe with as-grown CNTs (138.9 Ω mm^{-2} at 1 kHz) compared to that without CNTs (1086.6 Ω mm^{-2} at 1 kHz). Additionally, the
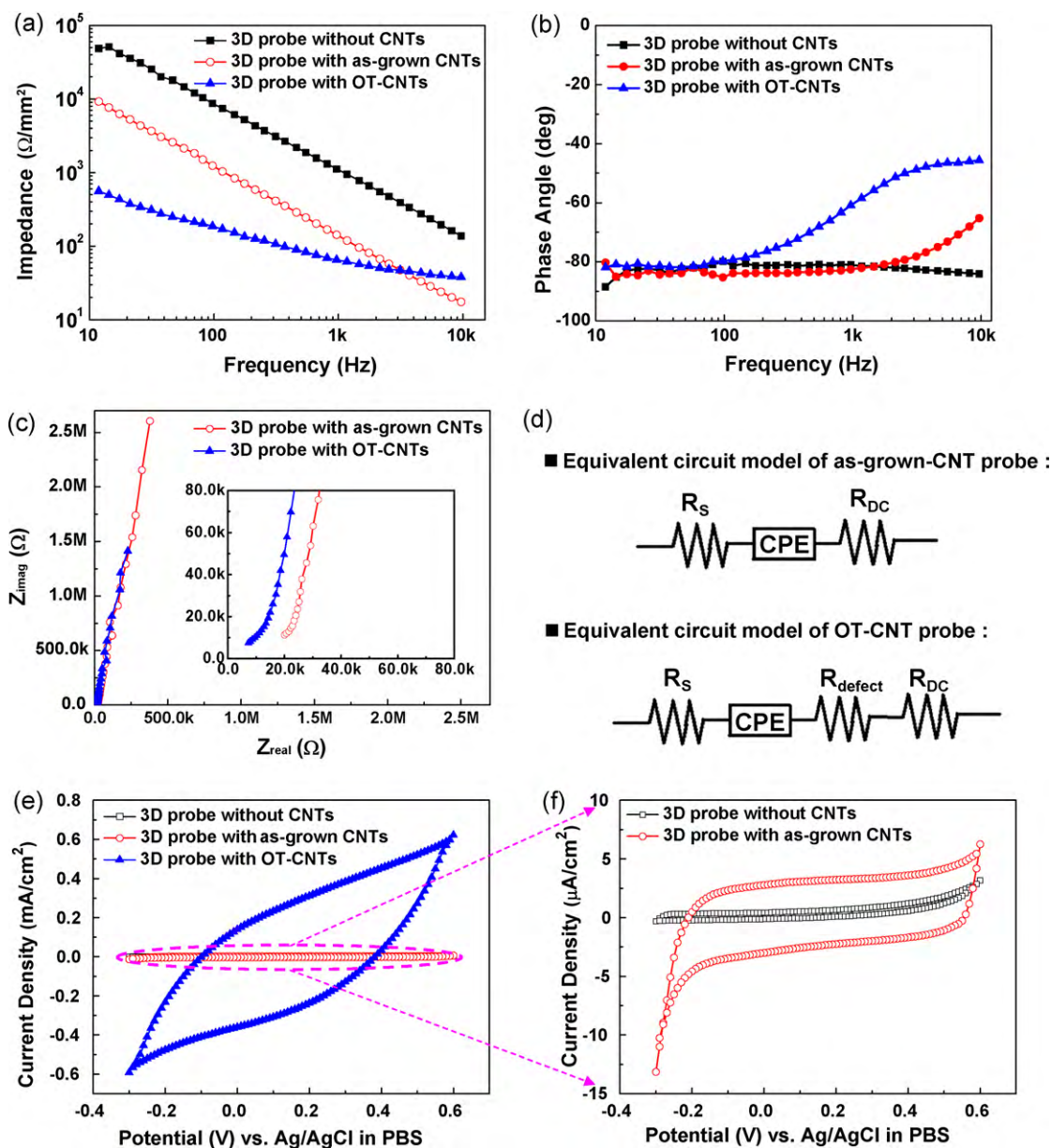
Fig. 4. (a) The interfacial impedance per unit area and (b) phase versus frequency of the 3D probes without CNTs, with as-grown CNTs, and with OT-CNTs over the frequency range of 10 Hz–10 kHz. (c) Nyquist plots of as-grown-CNT probe and OT-CNT probe and (d) the data fit to the equivalent circuit model. (e) Cyclic voltammogram of 3D probes without CNTs, with as-grown CNTs, and with OT-CNTs in PBS solution. The scan rate was 100 mV s^{-1}. (f) The enlarged CV data were taken from the dotted area in (e) (geometric area of probe of was about 10–2000 μm^2).

impedance per unit area dropped to 64.5 Ω mm^{-2} at 1 kHz for the OT-CNT probe (Fig. 4a). The results indicated that the existence of CNTs can decrease the impedance of the electrode. Furthermore, O_2 plasma treatment on CNTs can reduce the impedance further. It is suspected to be attributed to that O_2 plasma treatment can remove the a-C accumulated on CNT surface and also enhance the hydrophilicity of CNTs, resulting in most of the CNT surface area being accessible in aqueous solution. In addition, the impedance for the OT-CNT probes with different CNT densities and various amounts of CNTs were also discussed in Supplemental information Fig. S3. In Fig. 4b, the phases were −81.1° and −82.5° at 1 kHz for the 3D probes without CNTs and with as-grown CNTs, respectively, which all can be referred as capacitive impedance. However, the phase was −60° at 1 kHz for the OT-CNT probe, which represents the transmitted signals through both capacitive coupling and resistive conduction.

Fig. 4c shows the Nyquist plots of the AC impedance of the as-grown-CNT probe and OT-CNT probe measured in a frequency range from 10 Hz to 10 kHz, which exhibit a nearly straight line. The data could be fitted to equivalent circuit models of the as-grown-CNT probe and OT-CNT probe, respectively (Fig. 4d), where the interface between CNTs and PBS solution is represented by a constant phase element (CPE), R_S is the resistance of solution spreading, R_{DC} is the resistance of the 3D CNT probe, and R_{defect} is the resistance of defects caused by O_2 plasma treatment (Felten et al., 2005; Lee et al., 2005). The detailed discussion of above models is provided in Supplemental information.

Fig. 4e shows the CV data of the 3D probes without CNTs, with as-grown CNTs, and with OT-CNTs in PBS solution at a scan rate (v) of 100 mV s^{-1}. The magnified plots to observe more clearly for the former two probes are shown in Fig. 4f. The capacitance (C) was derived according to the following equation (Nguyen-Vu

et al., 2006), $C = \Delta i/2v$, where Δi is the current density deviation between the positive and negative voltage scan at the electrode–electrolyte interface. The voltammograms revealed featureless curves for the operational potential range, indicating no electrochemical activation and that the current was delivered from the interfacial capacitance. The interfacial capacitance per unit area derived from the CV data increased from $7\,\mu F\,cm^{-2}$ for the 3D probe without CNTs to greater than $29\,\mu F\,cm^{-2}$ for that with as-grown CNTs. Furthermore, the capacitance per unit area reached $2.5\,mF\,cm^{-2}$ for the OT-CNT probe, which was about two orders larger than that without O_2 plasma treatment. By benefitting from lower interfacial impedance and higher capacitance, the OT-CNT probe can enhance the electrical charge transfer characteristics and electrochemical properties, which can provide better sensitivity and facilitate their application for neural recording.

3.3. Neural signal recording of the 3D CNT probe

To demonstrate the capability of the as-grown-CNT probe and OT-CNT probe, they were employed to record the neural signals of a crayfish nerve cord. A diagram of the experimental setup is shown in Fig. 5a, where the as-grown-CNT probe or OT-CNT probe were contacting the membrane of the LG to record the neural responses. A twisted Teflon-coated Ag wire was placed on the mechanosensory primary afferent neurons for stimulation, and the Ag/AgCl electrode was immersed in buffer solution to ground the noise. The as-grown-CNT probe and OT-CNT probe were tightly attached to the LG axon, which were located on the dorsal surface of the nerve cord. The extracellular neural activities were difficult to be recorded by the as-grown-CNT probe, as shown in Supplemental information Fig. S4, while they can be detected by the OT-CNT probe as shown in Fig. 5b and c. According to Fig. 5b and c CNT probe was able to detect action potentials of the LG neurons. The recorded peak-to-peak magnitude of evoked action potentials was about 80.4 μV, and the root-mean-square (rms) of the noise voltage was about 1.9. The signal-to-noise ratio was about 42.3, which was obtained by dividing the peak-to-peak amplitude of the spike by the baseline of the recording trace for the OT-CNT probe with a pad area of 1500 μm^2.

Fig. 5d and e shows the equivalent circuit models of OT-CNT probe and as-grown-CNT probe, respectively, for LG neuron recording corresponding to Fig. 5a, where V_{in} is the action potential evoked from the LG neuron and V_{out} is the potential recorded by the CNT probe and amplified by the amplifier. The R_{seal} is the seal resistance between the LG neuron and the CNT probe (Massobrio et al., 2008). The Z_{CNT} represents the impedance of the CNT-electrolyte interface that can be modeled electrically as a resistor and a capacitor in parallel (Li et al., 2005; Yang et al., 2008). The Z_{SiO_2} and Z_{Si} are the impedance of the SiO_2–electrolyte interface and Si, respectively. The C_{SiO_2} presents the capacitance of SiO_2. Ideally, to achieve optimized neural signals, a minimized impedance of the electrode (Z_{CNT}) is required along with enough insulation to isolate the cs-Si

pad to avoid leakage current (Z_{SiO_2}). Additionally, the R_{seal} should be maximized to avoid signal loss. If the CNT probes contacting the LG neuron are not tight enough (R_{seal} is small), the CNT probe may not record the neural signal.

Comparisons of the equivalent circuit models between Fig. 5d and e also used to explain why it is critical to remove a-C on SiO_2. The neural signals were difficult to be recorded by the as-grown-CNT probe because of the conductive a-C accumulation on the SiO_2 surface of the probe. The resistance of the a-C (R_{a-C}) formed in parallel with the R_{seal} and V_{in}, where the evoked signals from the LG neuron would pass through the R_{a-C} to the ground. This would cause a leakage current when neural recording in buffer solution. If the a-C on SiO_2 was removed by O_2 plasma treatment, the R_{a-C} can be removed in the equivalent circuit. The signals from the LG neuron could directly pass through the Z_{CNT} to the amplifier. Based on above results, O_2 plasma treatment not only removed a-C on SiO_2 to avoid a leakage current, but also decreased the interfacial impedance of the CNT probe. The OT-CNT probe provides better charge transfer capability, which facilitates their application to neural recording.

3.4. Cone-shaped 3D CNT probe versus other CNT electrodes

A comparison of the performance of the 3D probes without CNTs, with as-grown CNTs, with OT-CNTs, and other CNT electrodes is summarized in Table 1. The impedance per unit area was lower and the capacitance per unit area was higher for the OT-CNT probe compared to those of the CNT microelectrodes (Wang et al., 2006) and SWCNT surface microelectrodes (Gabriel et al., 2009). It could be attributed to that more CNT surface area was accessible in aqueous solution since the 3D CNT probe exhibited the more spreading CNTs. The spreading CNTs easily become hydrophilic during O_2 plasma treatment for more effective O_2 plasma penetration into CNTs and more hydrophilic chemical bonds such as C–OH, C=O and OH–C=O were formed on the outermost surface of the CNTs. Above results suggest the superior impedance and capacitance characteristics are primarily contributed by the incremental C–OH, C=O and OH–C=O bonds which chemically anchor H_2O molecules via intermolecular bonding (Snow et al., 2005) and enhance the CNTs/electrolyte interfacial contact and reaction. In addition, the process time of O_2 plasma treatment to change the CNT surface from hydrophobic to hydrophilic (15 s) is much shorter compared to using incubation with PEG-PL for 2–20 h (Wang et al., 2006). Needle-shaped electrodes with several thousands μm in length, several hundreds μm in width, several tens μm in height have been reported (Kim et al., 1999; Wise, 2005). When compared these electrodes with several microelectrodes patterned on each shank of the structure that can provide higher density sensors, the 3D cone-shaped CNT probe presented in this work with several tens μm of heights and bottom diameters exhibits more surface contact area for neural recording at the same footprint area.

Table 1
Summary of the properties for cone-shaped (cs) 3D CNT probe fabricated in this work versus the works reported by other groups (Ø is the diameter of electrode, "Z" is the impedance, and "C" is the capacitance).

|	3D probe without CNTs	3D probe with as-grown CNTs	3D probe with O_2 plasma treated	CNT microelectrodes	SWCNT surface microelectrodes
Formation of CNT pad	–	Thermal CVD	Thermal CVD	Thermal CVD	Drop SWCNTs to electrode
Area of CNT pad (μm^2)	No CNT	10–2000	10–2000	30×30, Ø = 50	Ø = 40 m
Hydrophilic treatment	–	–	O_2 plasma treatment	PEG-PL	–
Contact angle (°)	–	146.3	3.5	–	–
"Z" per unit area ($\Omega\,mm^{-2}$)	1086.6	138.9	64.5	100	804.3
"C" per unit area ($mF\,cm^{-2}$)	0.007	0.029	2.5	1.6	4.59×10^{-5}
Peak-to-peak (μV)	–	–	80.4	–	210
Noise	–	–	1.9	–	–
Source	This work	This work	This work	Wang et al. (2006)	Gabriel et al. (2009)
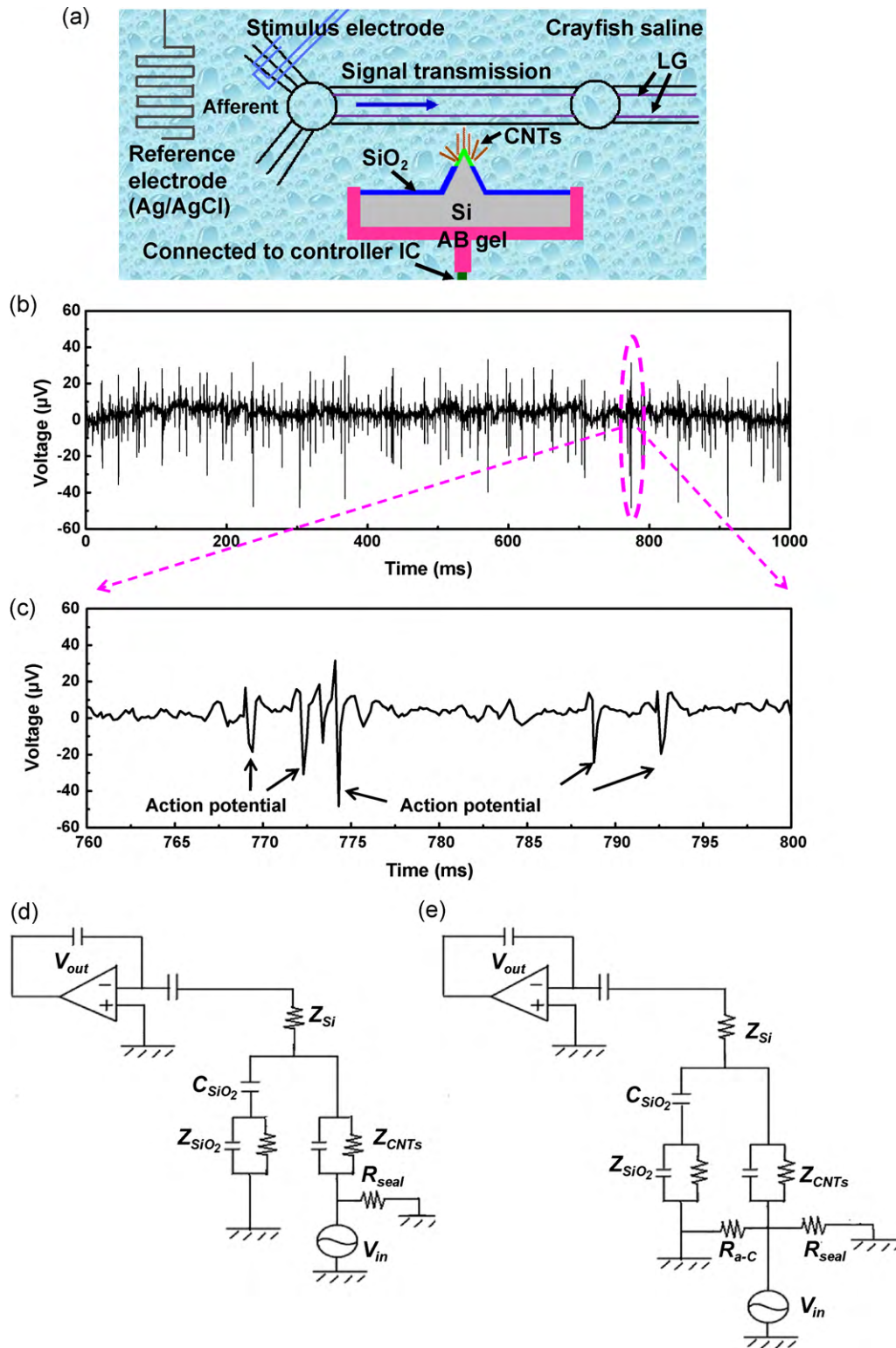
Fig. 5. (a) Diagram of the experimental setup using the 3D CNT probe for neural recording in the crayfish nerve cord. (b) The action potential of the crayfish nerve cord recorded by the OT-CNT probe, and (c) zoom-in image of the signals recorded by the OT-CNT probe from the dotted area in (b). (d) Schematic equivalent circuit model of using OT-CNT probes for neural recording in (a), and (e) schematic equivalent circuit model for as-grown-CNT probes.

The peak-to-peak voltage of the OT-CNT probe was smaller than SWCNT surface microelectrodes reported (Gabriel et al., 2009). As the recorded peak-to-peak voltage is dependent on the distance between the neuron and electrodes, further precise control on the distance is required for sensitivity comparison. However, the noise voltage of the probe immersing in the saline is determined by the resistance between saline and the CNT electrode, while independent of the distance between neuron and electrode. Instead, it relates to the characteristics of CNT electrode and the amplifier of instrument. The root-mean-square of the noise voltage was about 1.9 for the OT-CNT probe, which was lower than that of SWCNT surface microelectrodes (Gabriel et al., 2009). A lower value of root-

mean-square of noise voltage for the OT-CNT probe well explained the lower noises to be added on the signals recorded by OT-CNT probes. It demonstrated that the OT-CNT probe could minimize the noise and improve the recordings further.

The adhesion of CNTs onto the substrate was improved as it was critical for future long-term implantation and real-time recording applications. The forces applied by the neurons during the motion or the flowing of buffer solution are expected to be quite large, which would threaten the integrity of the CNT electrode and cause detachment of the CNTs from the substrate (Kotov et al., 2009). In Gabriel's SWCNT surface microelectrode, the SWCNTs attached to the Pt electrode by physical adsorption were easily detached from the substrate during cell culture (Gabriel et al., 2009). This easy detachment is an obstacle for long-term usage of CNT devices. In our 3D CNT probe, following CNT direct growth on the cs-Si tip by catalyst thermal CVD, a microwave (MW) treatment for 3 min at 900 W was also used to improve the adhesion of CNTs onto the substrates (Su et al., 2010). Hence, good adhesion of CNTs onto the substrate makes our 3D CNT probe a promising candidate for neural recording applications.

4. Conclusion

In conclusion, the feasibility of using a novel 3D cone-shaped (cs) CNT probe for extracellular neural recording has been demonstrated. The CNTs were grown on the cs-Si tip by catalytic thermal CVD. The 3D cone-shaped CNT probe exhibit a larger CNT surface area and higher spatial resolution of neural recording at the same footprint area compared to the planar-type CNT electrodes. The O_2 plasma treatment proposed in this work provides a simple way to make the surface of CNTs more hydrophilic. This surface change can enhance the electrical charge transfer characteristics and electrochemical properties of the OT-CNT probes attributed to the two-fold reduction of impedance and more than two orders of magnitude increase on interfacial capacitance compared to the as-grown-CNT probes. The superior electrochemical performance and good adhesion of the OT-CNT probe fabricated in this work make it is a promising candidate for neural recording applications.

Acknowledgments

Appendix A. Supplementary data

Supplementary data associated with this article can be found, in the online version, at doi:10.1016/j.bios.2010.06.015.

References

Campbell, P.K., Jones, K.E., Normann, R.A., 1990. Biomedical Sciences Instrumentation 26, 161–165.
Chapin, J.K., Moxon, K.A., Markowitz, R.S., Nicolelis, M., 1999. Nature Neuroscience 2 (7), 664–670.
Chen, C.H., Yao, D.J., Tseng, S.H., Lu, S.W., Chiao, C.C., Yeh, S.R., 2009. Biosensors and Bioelectronics 24 (7), 1911–1917.
Endo, M., Kim, Y.A., Fukai, Y., Hayashi, T., Terrones, M., Terrones, H., Dresselhaus, M.S., 2001. Applied Physics Letters 79 (10), 1531–1533.
Felten, A., Bittencourt, C., Pireaux, J.J., Van Lier, G., Charlier, J.C., 2005. Journal of Applied Physics 98 (7), 074308-1–9 (9 pp.).
Gabay, T., Ben-David, M., Kalifa, I., Sorkin, R., Abrams, Z.R., Ben-Jacob, E., Hanein, Y., 2007. Nanotechnology 18 (3), 035201-1–6 (6 pp.).
Gabriel, G., Gomez, R., Bongard, M., Benito, N., Fernandez, E., Villa, R., 2009. Biosensors and Bioelectronics 24 (7), 1942–1948.
Gheith, M.K., Pappas, T.C., Liopo, A.V., Sinani, V.A., Shim, B.S., Motamedi, M., Wicksted, J.P., Kotov, N.A., 2006. Advanced Materials 18 (22), 2975–2979.
Gooding, J.J., 2005. Electrochimica Acta 50 (15), 3049–3060.
Hochberg, L.R., Serruya, M.D., Friehs, G.M., Mukand, J.A., Saleh, M., Caplan, A.H., Branner, A., Chen, D., Penn, R.D., Donoghue, J.P., 2006. Nature 442, 164–171.
Hubel, D.H., 1957. Science 125, 549–550.
Keefer, E.W., Botterman, B.R., Romero, M.I., Rossi, A.F., Gross, G.W., 2008. Nature Nanotechnology 3, 434–439.
Keohan, F., Wei, X.F., Wongsarnpigoon, A., Lazaro, E., Darga, J.E., Grill, W.M., 2007. Journal of Biomaterials Science Polymer Edition 18 (8), 1057–1073.
Kim, Y.T., Kim, Y.Y., Jun, C.H., 1999. Proceedings of the Symposium on Design, Test, and Microfabrication of MEMS and MOEMS, vol. 3680, no. 2, Paris, France, pp. 924–930.
Kotov, N.A., Winter, J.O., Clements, I.P., Jan, E., Timko, B.P., Campidelli, S., Pathak, S., Mazzatenta, A., Lieber, C.M., Prato, M., Bellamkonda, R.V., Silva, G.A., Kam, N.W.S., Patolsky, F., Ballerini, L., 2009. Advanced Materials 21 (40), 3970–4004.
Krishnan, A., Dujardin, E., Ebbesen, T.W., Yianilos, P.N., Treacy, M.M.J., 1998. Physical Review B 58 (20), 14013–14019.
Lebedev, M.A., Nicolelis, M.A.L., 2006. Trends in Neurosciences 29 (9), 536–546.
Lee, J.S., Chandrashekar, A., Park, B.M., Overzet, L.J., Lee, G.S., 2005. Journal of Vacuum Science & Technology B 23 (3), 1013–1017.
Li, J., Ng, H.T., Cassell, A., Fan, W., Chen, H., Ye, Q., Koehne, J., Han, J., Meyyappan, M., 2003. Nano Letters 3 (5), 597–602.
Li, J., Koehne, J.E., Cassell, A.M., Chen, H., Ng, H.T., Ye, Q., Fan, W., Han, J., Meyyappan, M., 2005. Electroanalysis 17 (1), 15–27.
Li, P., Lim, X., Zhu, Y., Yu, T., Ong, C.K., Shen, Z., Wee, A.T.S., Sow, C.H., 2007. Journal of Physical Chemistry B 111 (7), 1672–1678.
Loeb, G.E., Peck, R.A., Martyniuk, J., 1995. Journal of Neuroscience Methods 63 (1–2), 175–183.
Lovat, V., Pantarotto, D., Lagostena, L., Cacciari, B., Grandolfo, M., Righi, M., Spalluto, G., Prato, M., Ballerini, L., 2005. Nano Letters 5 (6), 1107–1110.
Massobrio, G., Massobria, P., Martinoia, S., 2008. Nano Letters 8 (12), 4433–4440.
Mazzatenta, A., Giugliano, M., Campidelli, S., Gambazzi, L., Businaro, L., Markram, H., Prato, M., Ballerini, L., 2007. The Journal of Neuroscience 27 (26), 6931–6936.
Merabet, L.B., Rizzo, J.F., Amedi, A., Somers, D.C., Pascual-Leone, A., 2005. Nature Reviews Neuroscience 6, 71–77.
Musameh, M., Lawrence, N.S., Wang, J., 2005. Electrochemistry Communications 7 (1), 14–18.
Navarro, X., Krueger, T.B., Lago, N., Micera, S., Stieglitz, T., Dario, P., 2005. Journal of the Peripheral Nervous System 10, 229–258.
Nguyen-Vu, T.D.B., Chen, H., Cassell, A.M., Andrews, R., Meyyappan, M., Li, J., 2006. Small 2 (1), 89–94.
Normann, R.A., 2007. Nature Clinical Practice Neurology 3 (8), 444–452.
Okpalugo, T.I.T., Papakonstantinou, P., Murphy, H., McLaughlin, J., Brown, N.M.D., 2005. Carbon 43 (1), 153–161.
Patolsky, F., Timko, B.P., Yu, G., Fang, Y., Greytak, A.B., Zheng, G., Lieber, C.M., 2006. Science 313, 1100–1104.
Schwartz, A.B., Cui, X.T., Weber, D.J., Moran, D.W., 2006. Neuron 52 (1), 205–220.
Shanmugam, S., Gedanken, A., 2006. Electrochemistry Communications 8 (7), 1099–1105.
Snow, E.S., Perkins, F.K., Houser, E.J., Badescu, S.C., Reinecke, T.L., 2005. Science 307, 1942–1945.
Su, H.C., Chen, C.H., Chen, Y.C., Yao, D.J., Chen, H., Chang, Y.C., Yew, T.R., 2010. Carbon 48 (3), 805–812.
Taylor, D.M., Tillery, S.I., Schwartz, A.B., 2002. Science 296, 1829–1832.
Tseng, S.H., Tsai, L.Y., Yeh, S.R., 2008. The Journal of Neuroscience 28 (28), 7165–7173.
Wang, K., Fishman, H.A., Dai, H., Harris, J.S., 2006. Nano Letters 6 (9), 2043–2048.
Wise, K.D., 2005. Engineering in Medicine and Biology Magazine IEEE 24 (5), 22–29.
Yang, S., Huo, J., Song, H., Chen, X., 2008. Electrochimica Acta 53 (5), 2238–2244.
Yeh, S.R., Chen, Y.C., Su, H.C., Yew, T.R., Kao, H.H., Lee, Y.T., Liu, T.A., Chen, H., Chang, Y.C., Chang, P., Chen, H., 2009. Langmuir 25 (13), 7718–7724.